

SHAPE AND THERMAL MODELING OF A SELECTION OF M-TYPE ASTEROIDS. K. T. Crane¹ (kcrane1@utk.edu), J. P. Emery¹ (jemery2@utk.edu), L. F. Lim², ¹Department of Earth and Planetary Sciences, University of Tennessee, Knoxville, 37996, ²NASA Goddard Space Flight Center (Lucy.F.Lim@nasa.gov)

Introduction: Tholen M-type asteroids exhibit featureless visible wavelength spectra and have a range of radar albedos. Since metallic iron shares these properties, and since iron meteorites are commonly found on Earth (and even Mars), it has long been assumed that at least some M-types possess metallic compositions [1]. More recent observations have revealed greater mineralogical variability in their compositions. Several M-type asteroids have 3 μm absorption features, indicating the presence of hydroxides and phyllosilicates [2]. Many also exhibit an absorption feature near 0.9 μm suggesting orthopyroxene and clinopyroxene surface compositions [3]. High radar albedos of 7 M-types suggest a significant metal fraction at the surface (high regolith bulk density), whereas moderate radar albedos of 10 others are consistent with silicate surfaces [4]. With such a variety of surface properties, the question remains: which if any M-type asteroids are the metallic cores of differentiated asteroids?

Asteroids with metal-rich surfaces should have high thermal inertias as well as weak or absent silicate emission features in the mid-infrared (~ 10 and $20 \mu\text{m}$). To test this hypothesis, we investigate their thermal and physical properties (thermal inertia, roughness, albedo, etc.) using thermal emission spectra measured with the Spitzer space telescope. Initial analysis of the 27 asteroids in the Spitzer sample revealed 6 asteroids with data suggestive of high thermal inertia [5]. These six asteroids are 216 Kleopatra, 796 Sarita, 497 Iva, 184 Dejopeja, 771 Libera, and 125 Liberatrix. Here, we include a more accurate shape determination of these asteroids in thermophysical models of the thermal emission data.

Observations: The spectra were measured using the Infrared Spectrograph (IRS) on the Spitzer space telescope as part of a program that included 27 M-type asteroids. IRS covers the spectral range 5.2–38 μm in four low-resolution (R~64-128) modules. Two high resolution (R~600) modules operate from 9.9–37 μm . All objects were observed with the short wavelength (SL; $\lambda < 14.2 \mu\text{m}$) modules. Fifteen of the objects in the full program were too bright for the long-wavelength (LL; $\lambda > 14.2 \mu\text{m}$) low-resolution modules, so these were observed with the high-resolution mode (SH, LH). The SH module overlaps with the SL1 module from 9.9 to 14.2 μm , providing confirmation of spectral features detected in this important re-

gion on the long wavelength edge of the silicate resonance band near 10 μm . Of the six asteroids studied here, Sarita, Iva, and Libera were observed solely in low-res mode (SL and LL), whereas Kleopatra, Dejopeja, and Liberatrix were observed in the hi-res mode longward of 10 μm (SL, SH, LH) wavelengths (SL, SH, and LH).

Shape Modeling: Each asteroid shape is defined using vertices and facets, with each vertex making six triangular facets by connecting lines with its six nearest neighbor vertices. Facets represent areas of equal elevation on the asteroid's surface and are therefore not necessarily of constant size or shape. These data were taken from the Planetary Data Systems collection of Hudson Shape Models (216 Kleopatra) and from Database of Asteroid Models from Inversion Techniques (184 Dejopeja, 771 Libera, 125 Liberatrix). (*Note:* Representative ellipsoid models are used for 796 Sarita and 497 Iva, as compilations of vertices and facets were unavailable.) Rotations about the z- and x-axes and specified viewing dimensions allow for the asteroids to be viewed from the observer or the sun in accordance with their spin pole determinations and periods. Because the surfaces are represented by triangular facets, normal vectors, surface areas for each facet, and projected surface area toward any target are all optional and useful calculations. These parameters are later used in the thermal modeling aspects. Using observer-centric ecliptic latitude and longitude and helio-centric latitude and longitude, vectors from the sun and observer to the center of the asteroid are also calculated.

Thermal Modeling: The asteroids' albedo, distance from the sun, distance from the observer, emissivity, and rotation state are used to calculate the temperature of each facet. Previous analyses of these data [5] used the NEATM [6], a slight modification of the Standard Thermal Model [7], which assumes a spherical shape, giving a temperature distribution of the form

$$T(i) = T_{ss} \cos^{1/4}(i)$$

where T_{ss} is the sub-solar temperature and i is the incidence angle (or angle from the sub-solar point). In the present work, we incorporate real, non-spherical shapes. Our modeling is completed in two stages. The first can be thought of as a non-spherical NEATM, in

which temperature is calculated from energy conservation at the surface for each facet, with a “beaming parameter” incorporated to account for the combined effects of thermal inertia and surface roughness. The second stage uses a thermophysical model that explicitly considers heat conduction and surface roughness as well as non-spherical shapes.

The bolometric bond albedo, which is a critical parameter for energy balance, is calculated using

$$A = pq$$

and

$$q = 0.29 + 0.684 G$$

where p represents geometric albedo, q is the bolometric phase integral, and G is the slope parameter [8]. Distances and asteroid-target angles are taken from the Horizons database, emissivity is assumed to be 0.9 for each asteroid.

The thermal flux of each facet “facing” the observer is calculated from the Planck function for the temperature and projected area of the given facet. The flux from all visible facets are then summed to provide an estimation of total flux projected toward the observer, like an approximate integral over an irregular surface. Note that to be “facing” the observer means that the facet in question has a normal vector to its surface less than 90° from the observer-asteroid vector calculated in the shape modeling portion of the program. This disk-integrated model flux is compared to the flux

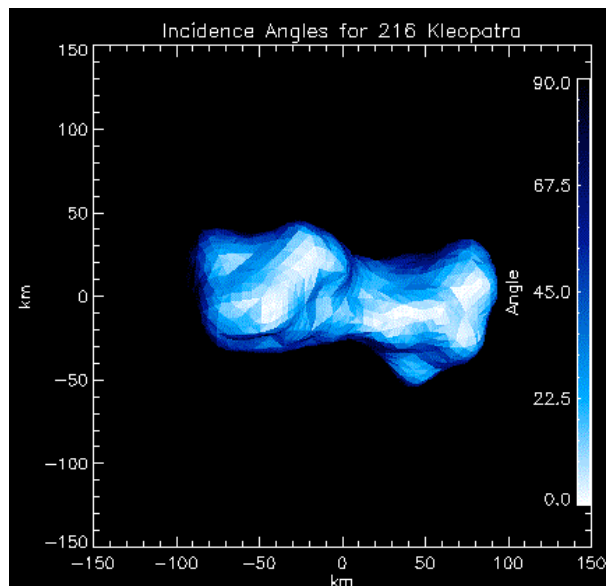


Figure 1. Colored surface of 216 Kleopatra with “whiter” colors representing surfaces with high incidence angles and “bluer” colors representing surfaces with lower incidence angles.

measured by Spitzer for each asteroid. Physical parameters (e.g., size, thermal inertia) are varied to find the best match between the data and model.

For display, the surface is colored according to the emission angle, incidence angle, thermal flux, or sub-

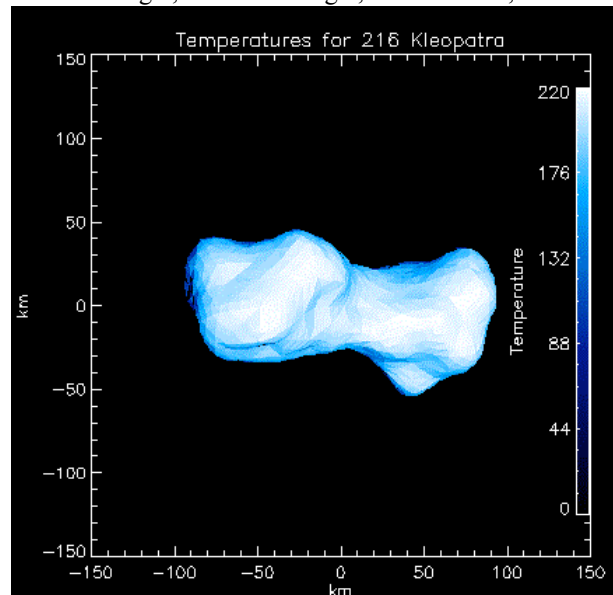


Figure 2. Colored surface of 216 Kleopatra with “whiter” colors representing surfaces with high temperatures and “bluer” colors representing surfaces with lower temperatures.

solar temperature of each facet. For example, in Figure 1, 216 Kleopatra is plotted and colored based on incidence angle and in Figure 2 is plotted using temperature data. Since incidence angle is the angle between each facet’s normal vector and the sun-asteroid vector and temperature is a function of sub-solar angle, it is clear how these plots correlate.

Results: Determinations of six Tholen M-type asteroids’ shapes are calculated, and surfaces representative of the thermal properties of each asteroid are modeled providing a unique insight into these likely candidates for metallicly composed main-belt asteroids amongst their more-likely mineralogically variable M-type counterparts.

References: [1] Fornasier S. et al. (2010) *Icarus*, 214, 1. [2] Rivkin A. S. et al. (2000) *Icarus*, 145, 351-368. [3] Hardersen P.S. et al. (2011) *Meteoritics & Planet. Sci.*, 46, 12. [4] Shepard M. K. et al. (2010) *Icarus*, 208, 221-237. [5] Emery, J.P. and Lim, L.F. (2011) *43rd DPS*, abstract #1438. [6] Harris, A.W. (1998) *Icarus* 131, 291-301. [7] Lebofsky L. A. and Spencer J. R. (1988) *Asteroids II*, 128-147. [8] Tedesco E. F. (1988) *Asteroids II*, 1090-1139.